Charmless B to PP,PV, VV decays Based on the Six-quark Effective Hamiltonian with Strong Phase

Ci Zhuang in collaboration with Su Fang, Y.L.Wu, Y.B.Yang

J.Phys.G38:015006,2011; Int.J.Mod.Phys.A25:69-111,2010;

KITPC/ITP-CAS

Outline

Four-quark operator effective Hamiltonian

$$H_{\rm eff} = \frac{G_F}{\sqrt{2}} \sum_{q=u,c} \lambda_q^s \left[C_1(\mu) O_1^{(q)}(\mu) + C_2(\mu) O_2^{(q)}(\mu) + \sum_{i=3}^{10} C_i(\mu) O_i(\mu) \right] + \text{h.c.} ,$$

where $\lambda_q^s = V_{qb} V_{qs}^*$ are products of the CKM matrix elements, $C_i(\mu)$ the Wilson coefficient functions, and $O_i(\mu)$ the four-quark operators

$$O_1^{(q)} = (\bar{q}_i b_i)_{V-A} (\bar{s}_j q_j)_{V-A} , \qquad O_2^{(q)} = (\bar{s}_i b_i)_{V-A} (\bar{q}_j q_j)_{V-A} ,$$

$$O_3 = (\bar{s}_i b_i)_{V-A} \sum_{q'} (\bar{q}'_j q'_j)_{V-A} , \qquad O_4 = \sum_{q'} (\bar{q}'_i b_i)_{V-A} (\bar{s}_j q'_j)_{V-A} ,$$

$$O_5 = (\bar{s}_i b_i)_{V-A} \sum_{q'} (\bar{q}'_j q'_j)_{V+A} , \qquad O_6 = -2 \sum_{q'} (\bar{q}'_i b_i)_{S-P} (\bar{s}_j q'_j)_{S+P} ,$$

$$O_7 = \frac{3}{2} (\bar{s}_i b_i)_{V-A} \sum_{q'} e_{q'} (\bar{q}'_j q'_j)_{V+A} , \qquad O_8 = -3 \sum_{q'} e_{q'} (\bar{q}'_i b_i)_{S-P} (\bar{s}_j q'_j)_{S+P} ,$$

$$O_9 = \frac{3}{2} (\bar{s}_i b_i)_{V-A} \sum_{q'} e_{q'} (\bar{q}'_j q'_j)_{V-A} , \qquad O_{10} = \frac{3}{2} \sum_{q'} e_{q'} (\bar{q}'_i b_i)_{V-A} (\bar{s}_j q'_j)_{V-A} .$$

Motivation of six-quark

1. Meson:
   Quark-antiquark bound state;
2. B decays to two light mesons:
   Three quark-antiquark pairs;
3. Leading order:
   One W boson and one gluon exchange;
4. The four quarks via W-boson exchange can be regarded as a local four quark interaction at the energy scale much below the W-boson mass, while two QCD vertexes due to gluon exchange are at the independent space-time points, the resulting effective six quark operators are hence in general nonlocal;

Six-quark operators

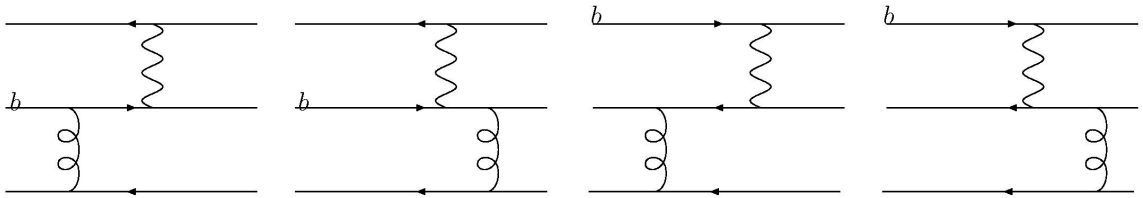

Figure:
Four different six-quark diagrams with a single W-boson exchange and a single gluon exchange

For example, the operator corresponding to the second diagram can be written as:

$$O_{q_2}^{(6)} = 4\pi\alpha_s \int\int \frac{\mathrm{d}^4k}{(2\pi)^4}\frac{\mathrm{d}^4p}{(2\pi)^4} e^{-i((x_1-x_2)p+(x_2-x_3)k)}(\bar{q}'(x_3)\gamma_\nu T^a q'(x_3))\frac{1}{k^2+i\epsilon}$$
$$(\bar{q}_2(x_2)\frac{\not{p}+m_{q_1}}{p^2-m_{q_1}^2+i\epsilon}\gamma^\nu T^a\Gamma_1 q_1(x_1))*(\bar{q}_4(x_1)\Gamma_2 q_3(x_1)),$$

1. The full operators of six-quark shall sum over the four diagrams:

$$O^{(6)} = \sum_{j=1}^{4} O_{q_j}^{(6)}.$$

2. Actually, the initial six quark operators $O_{q_j}^{(6)}(j = 1, 2, 3, 4)$ can be obtained from the following initial four quark operator via a single gluon exchange:

$$O \equiv (\bar{q}_2 \Gamma_1 q_1) * (\bar{q}_4 \Gamma_2 q_3)$$

The possible six-quark diagrams at one loop level

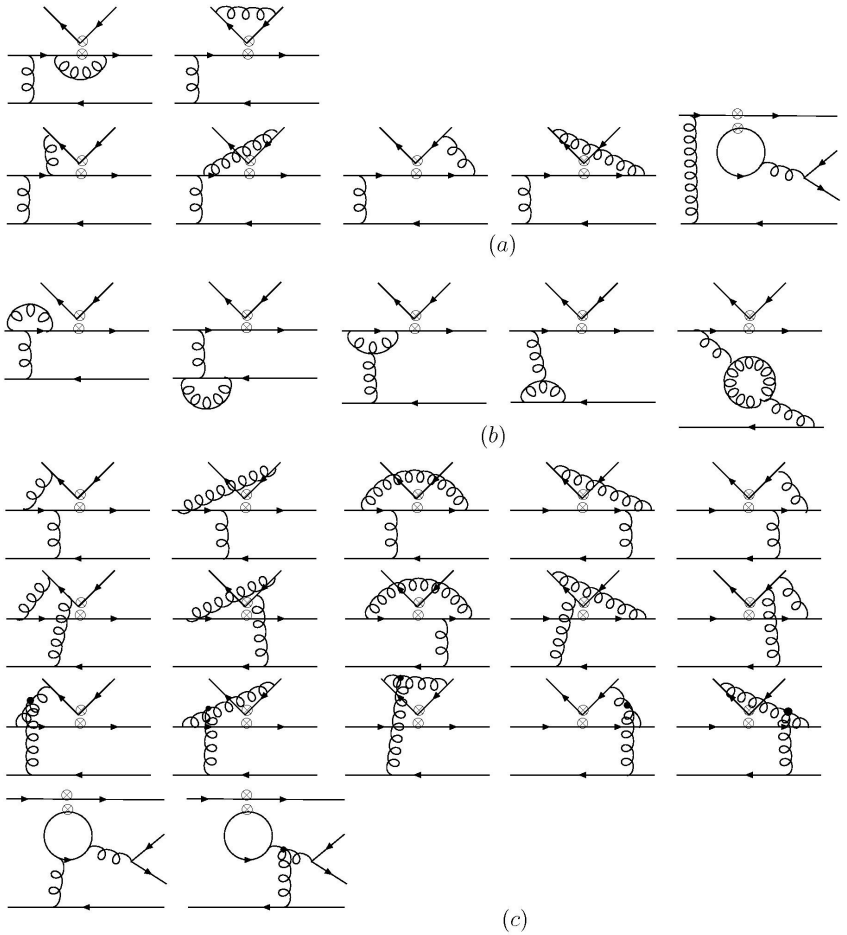

(a)One-Loop contributions only to the effective weak vertex(type I).

(b)One-Loop contributions only to the gluon vertexes (type II).

(c)One-Loop contributions for both weak and strong vertexes (type III).

When ignoring the type III diagrams, we arrive at an approximate six quark operator effective Hamiltonian as follows:

$$\begin{aligned} H_{\rm eff}^{(6)} &= \frac{G_F}{\sqrt{2}} \sum_{j=1}^{4} \{ \sum_{q=u,c} \lambda_q^{s(d)} [C_1(\mu) O_{1q_j}^{(q)(6)}(\mu) + C_2(\mu) O_{2q_j}^{(q)(6)}(\mu)] \\ &+ \sum_{i=3}^{10} \lambda_t^{s(d)} C_i(\mu) O_{i\ q_j}^{(6)}(\mu) \} + h.c. + \ldots, \end{aligned}$$

with:

$$O_{i\ q_j}^{(6)}(\mu)(j = 1, 2, 3, 4)$$

are six quark operators which may effectively be obtained from the corresponding four quark operators $O_i(\mu)(i = 1 - 10)$ at the scale μ via the effective gluon exchanging interactions between one of the external quark lines of four quark operators and a spectator quark line at the same scale μ.

From six-quark operators to hadronic matrix elements

For example, we examine the hadronic matrix elements of $B \to \pi^0\pi^0$ decay for a typical six-quark operator $O_{LL}^{(6)}$:

$$\begin{aligned} O_{LL}^{(6)} \quad = \quad & \int\int \frac{\mathrm{d}^4 k}{(2\pi)^4} \frac{\mathrm{d}^4 p}{(2\pi)^4} e^{-i((x_1-x_2)p+(x_2-x_3)k)} \frac{1}{k^2} \frac{1}{p^2-m_d^2} \\ & [\bar{d}_k(x_2)(\not{p}+m_d)\gamma^\nu T^a_{ki}\gamma^\mu(1-\gamma^5)b_i(x_1)] \\ & [\bar{d}_j(x_1)\gamma_\mu(1-\gamma^5)d_j(x_1)][\bar{d}_m(x_3)\gamma_\nu T^a_{mn}d_n(x_3)], \end{aligned}$$

which is actually a part of the six quark operator $O_{4q_2}^{(6)}$ in the effective Hamiltonian. Its hadronic matrix elements are the most abundant for $B \to \pi^0\pi^0$ decay.

Reduction of hadronic matrix elements

Its hadronic matrix element for $B \to \pi^0\pi^0$ decay leads to the following most general terms in the QCD factorization approach:

$$
\begin{aligned}
M_{LL}^{O}(B\pi\pi) \equiv & < \pi^0\pi^0 \mid O_{LL}^{(6)} \mid \bar{B}_0 > \\
= & \int\int \frac{\mathrm{d}^4k}{(2\pi)^4} \frac{\mathrm{d}^4p}{(2\pi)^4} e^{-i((x_1-x_2)p+(x_2-x_3)k)} \frac{1}{k^2} \frac{1}{p^2-m_d^2} \\
& < \pi^0\pi^0 \mid [\bar{d}_k(x_2)(\not{p}+m_d)\gamma^\nu T^a_{ki}\gamma^\mu(1-\gamma^5)b_i(x_1)] \\
& [\bar{d}_j(x_1)\gamma_\mu(1-\gamma^5)d_j(x_1)][\bar{d}_m(x_3)\gamma_\nu T^a_{mn}d_n(x_3)] \mid \bar{B}_0 > \\
\equiv & M_{LL}^{O(1)} + M_{LL}^{O(2)} + M_{LL}^{O(3)} + M_{LL}^{O(4)},
\end{aligned}
$$

$M_{LL}^{O(i)}(i = 1, 2, 3, 4)$ correspond to the four different diagrams of reduction:

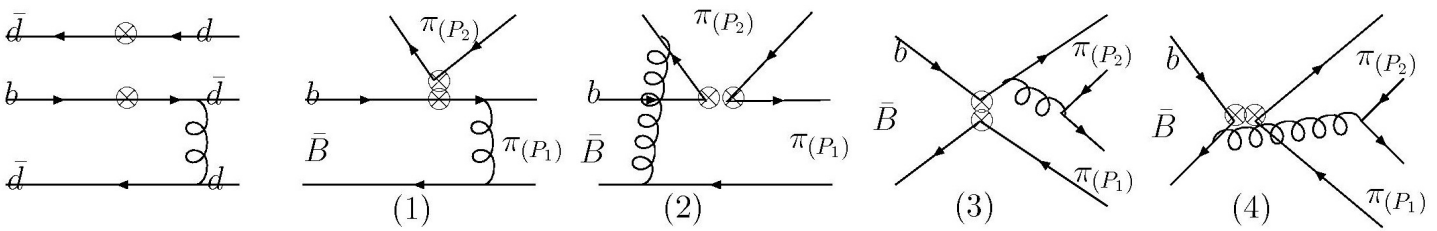

Figure: *Different ways of reducing hadronic matrix element by QCDF*

Explicit structure of MLL

For example, the expression of $M_{LL}^{O(1)}$ is as follows:

$$M_{LL}^{O(1)} = \int\int \frac{d^4k}{(2\pi)^4}\frac{d^4p}{(2\pi)^4} e^{-i((x_1-x_2)p+(x_2-x_3)k)} \frac{1}{k^2(p^2-m_d^2)} T^a_{ki} T^a_{mn}$$
$$[(\not{p}+m_d)\gamma^\nu\gamma^\mu(1-\gamma^5)]_{\rho\sigma}[\gamma_\mu(1-\gamma^5)]_{\alpha\beta}[\gamma_\nu]_{\gamma\delta} M_{Bim}^{\sigma\gamma}(x_1,x_3) M_{\pi nk}^{\delta\rho}(x_3,x_2) M_{\pi jj}^{\beta\alpha}(x_1,x_1),$$

with:

$$\begin{aligned} M_{Bnm}^{\beta\alpha}(x_i,x_j) &= <0 \mid \bar{d}_m^\alpha(x_j) b_n^\beta(x_i) \mid \bar{B}^0(P_B)> \\ &= -\frac{iF_B}{4}\frac{\delta_{mn}}{N_c}\int_0^1 du\, e^{-i(u\,P_B^+ x_j + (P_B - u\,P_B^+)\,x_i)} M_{\rm B}^{\beta\alpha}(u,P_B), \\ M_{\pi nm}^{\beta\alpha}(x_i,x_j) &= <\pi^0(P) \mid \bar{d}_m^\alpha(x_j) d_m^\beta(x_i) \mid 0> = \frac{iF_\pi}{4}\frac{\delta_{mn}}{N_c}\int_0^1 dx\, e^{-i(x\,P\,x_j + (1-x)P\,x_i)} M_\pi^{\beta\alpha}(x,P), \end{aligned}$$

with F_M $(M = B, \pi)$ the decay constants. Here $M_{\rm B}^{\beta\alpha}(u,P_B)$ and $M_\pi^{\beta\alpha}(x,P)$ are the spin structures for the bottom meson and light meson π and characterized by the corresponding distribution amplitudes.

After performing the integration over space-time and momentum, the amplitude is simplified to be:

$$M^{O}_{LL}(B\pi\pi) =< \pi^0\pi^0 \mid O^{(6)}_{LL} \mid \bar{B}_0 >= \int_0^1\int_0^1\int_0^1 du\,dx\,dy$$

$$\{\frac{1}{(u\,P_B^+ - (1-x)P_1)^2}[\frac{M^{(1)}_{LL}}{(P_1 - u\,P_B^+)^2 - m_d^2} + \frac{M^{(2)}_{LL}}{((1-x)P_1 + y\,P_2 - u\,P_B^+)^2 - m_d^2}]$$

$$+ \quad \frac{1}{(xP_1 + (1-y)P_2)^2}[\frac{M^{(3)}_{LL}}{(x\,P_1 + P_2)^2 - m_d^2} + \frac{M^{(4)}_{LL}}{(x\,P_1 + (1-y)P_2 - u\,P_B^+)^2 - m_d^2}]\},$$

with:

$$M^{(1)}_{LL} = \frac{C_F}{N_C} * F_B\ F_\pi^2 \mathrm{Tr}[M_B(u,P_B)\gamma_\nu M_\pi(x,P_1)\gamma^\nu(\not{P}_1 - u\not{P}_B^+ + m_d)\gamma_\mu(1-\gamma^5)]$$

$$\mathrm{Tr}[M_\pi(y,P_2)\gamma^\mu(1-\gamma^5)] = i\frac{C_F}{4N_C}F_B\ F_\pi^2\phi_B(u)m_B^3\mu_\pi\phi_\pi(y)\phi_\pi^p(x),$$

.....

where $M^{(i)}_{LL}(i = 1,2,3,4)$ are obtained by performing the trace of matrices and determined by the distribution amplitudes.

Four kinds of diagrams

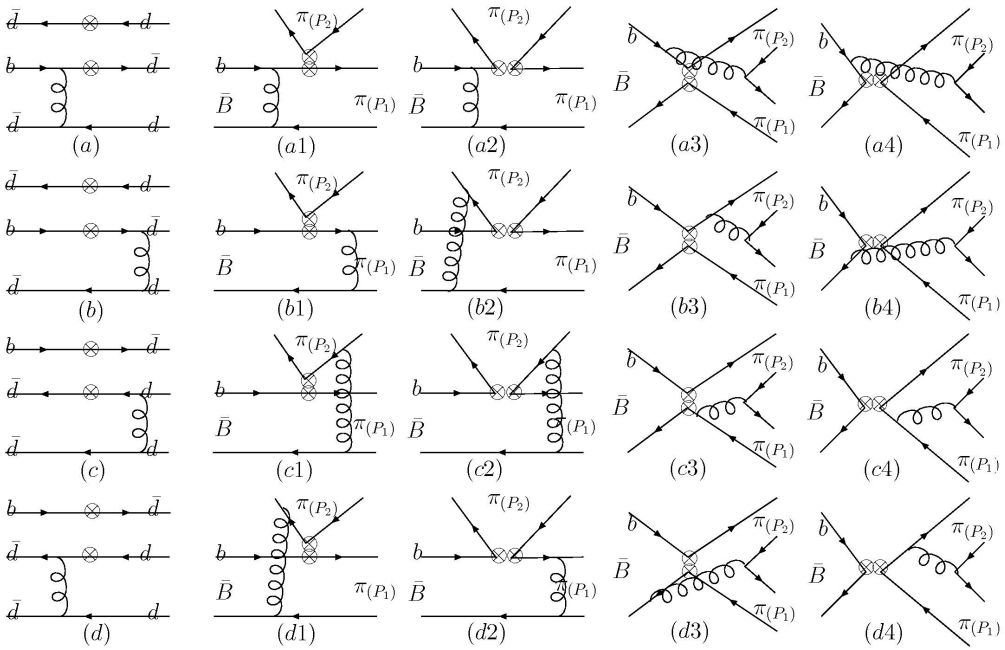

Figure: *Four types of effective six quark diagrams lead to sixteen diagrams for hadronic two body decays of heavy meson via QCD factorization*

The first diagram is known as the **factorizable one**, the second is the **non-factorizable one** and color suppressed. The third is the **factorizable annihilation diagram and color suppressed**, and the fourth is an **annihilation diagram and its matrix element vanishes**.

Independent terms

The effective four quark vertexes concern three types of current-current interactions: $(V-A)\times(V-A)$ or (LL), $(V-A)\times(V+A)$ or (LR), $(S-P)\times(S+P)$ or (SP). Therefore, there are totally $4\times4\times3$ kinds of hadronic matrix elements involved in the QCD factorization approach, while only half of them are independent with the following relations:

$$
\begin{array}{llllllllllll}
M_{LL}^{a1} = T_{LLa}^{F}; & M_{LL}^{a2} = T_{LLa}^{F}/N_C; & M_{LL}^{a3} = A_{LLa}^{N}/N_C; & M_{LL}^{a4} = 0; \\
M_{LR}^{a1} = T_{LRa}^{F}; & M_{LR}^{a2} = T_{SPa}^{F}/N_C; & M_{LR}^{a3} = A_{SPa}^{N}/N_C; & M_{LR}^{a4} = 0; \\
M_{SP}^{a1} = T_{SPa}^{F}; & M_{SP}^{a2} = T_{LRa}^{F}/N_C; & M_{SP}^{a3} = A_{LRa}^{N}/N_C; & M_{SP}^{a4} = 0; \\
M_{LL}^{b1} = T_{LLb}^{F}; & M_{LL}^{b2} = T_{LLb}^{N}/N_C; & M_{LL}^{b3} = A_{LLb}^{F}/N_C; & M_{LL}^{b4} = 0; \\
M_{LR}^{b1} = T_{LRb}^{F}; & M_{LR}^{b2} = T_{SPb}^{N}/N_C; & M_{LR}^{b3} = A_{SPb}^{F}/N_C; & M_{LR}^{b4} = 0; \\
M_{SP}^{b1} = T_{LLb}^{F}; & M_{SP}^{b2} = T_{LRb}^{N}/N_C; & M_{SP}^{b3} = A_{LRb}^{F}/N_C; & M_{SP}^{b4} = 0; \\
M_{LL}^{c1} = 0; & M_{LL}^{c2} = T_{LLa}^{N}/N_C; & M_{LL}^{c3} = A_{LLa}^{F}/N_C; & M_{LL}^{c4} = A_{LLa}^{F}; \\
M_{LR}^{c1} = 0; & M_{LR}^{c2} = T_{SPa}^{N}/N_C; & M_{LR}^{c3} = A_{SPa}^{F}/N_C; & M_{LR}^{c4} = A_{LRa}^{F}; \\
M_{SP}^{c1} = 0; & M_{SP}^{c2} = T_{LRa}^{N}/N_C; & M_{SP}^{c3} = A_{LRa}^{F}/N_C; & M_{SP}^{c4} = A_{SPa}^{F}; \\
M_{LL}^{d1} = 0; & M_{LL}^{d2} = T_{LLb}^{F}/N_C; & M_{LL}^{d3} = A_{LLb}^{N}/N_C; & M_{LL}^{d4} = A_{LLb}^{F}; \\
M_{LR}^{d1} = 0; & M_{LR}^{d2} = T_{SPb}^{F}/N_C; & M_{LL}^{d3} = A_{SPb}^{N}/N_C; & M_{LL}^{d4} = A_{LRb}^{F}; \\
M_{SP}^{d1} = 0; & M_{SP}^{d2} = T_{LRb}^{F}/N_C; & M_{LL}^{d3} = A_{LRb}^{N}/N_C; & M_{LL}^{d4} = A_{SPb}^{F}.
\end{array}
$$

Treatment of Singularities

There are two kinds of singularities in the evaluation of hadronic matrix elements:

- Infrared divergence of gluon exchanging interaction
- On mass-shell divergence of internal quark propagator

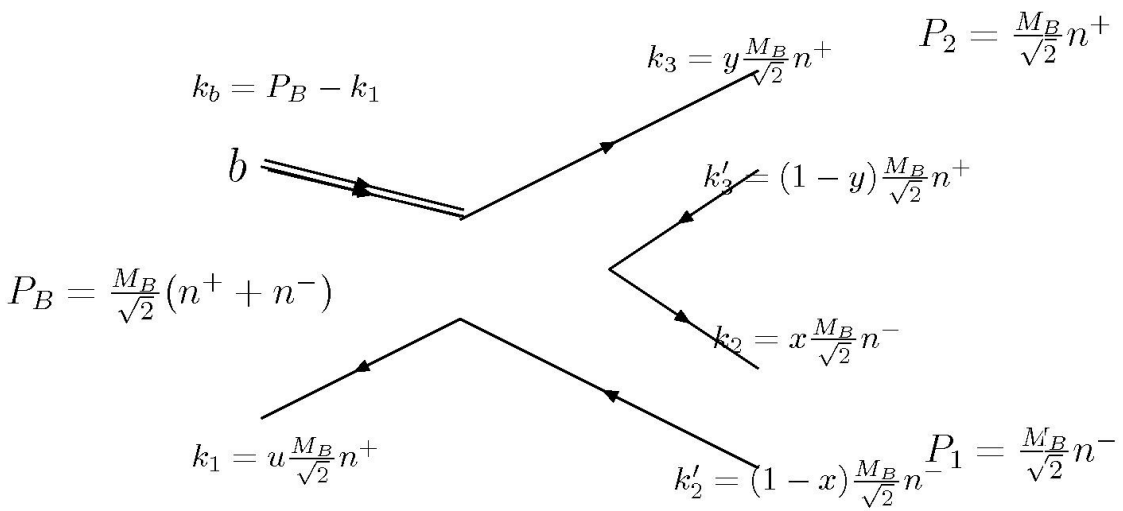

Figure: *Definition of momentum in* $B \to M_1 M_2$ *decay. The light-cone coordinate is adopted with* $(n^+, n^-, \vec{k}_\perp)$.

Treatment of Singularities

1. **Quark propagator**
   Applying the Cutkosky rule to deal with a physical-region singularity of all propagators, the following formula holds:

$$\frac{1}{p^2 - m_q^2 + i\epsilon} = P\left[\frac{1}{p^2 - m_q^2}\right] - i\pi\delta[p^2 - m_q^2],$$

   which is known as the principal integration method, and the integration with the notation of capital letter P is the so-called principal integration.

2. **Gluon propagator**
   We prefer to add the same dynamics mass for both gluon and light quark to investigate the infrared cut-off dependence of perturbative theory prediction:

$$\frac{1}{k^2}\frac{\not{p} + m_q}{(p^2 - m_q^2)} \quad \rightarrow \quad \frac{1}{(k^2 - \mu_g^2 + i\epsilon)}\frac{\not{p} + \mu_q}{(p^2 - \mu_q^2 + i\epsilon)} \text{ (q is a light quark).}$$

   Here the energy scale μ_g, μ_q plays the role of infrared cut-off but preserving gauge symmetry and translational symmetry of original theory.Use of this effective gluon propagator is supported by the lattice and the field theoretical studies, which have shown that the gluon propagator is not divergent as fast as $\frac{1}{k^2}$.

Applying this prescription to the amplitude illustrated in previous section, we have

$$M_{LL}^{O}(B\pi\pi) =< \pi^0\pi^0 \mid O_{LL}^{(6)} \mid \bar{B}_0 >= \int_0^1\int_0^1\int_0^1 du\,dx\,dy$$

$$\{\frac{1}{(u\,P_B^+ - (1-x)P_1)^2 - \mu_g^2 + i\epsilon}[\frac{M_{LL}^{(1)}}{(P_1 - u\,P_B^+)^2 - m_q^2 + i\epsilon}$$

$$+\frac{M_{LL}^{(2)}}{((1-x)P_1 + y\,P_2 - u\,P_B^+)^2 - m_q^2 + i\epsilon}]$$

$$+\frac{1}{(xP_1 + (1-y)P_2)^2 - \mu_g^2 + i\epsilon}[\frac{M_{LL}^{(3)}}{(x\,P_1 + P_2)^2 - m_q^2 + i\epsilon}$$

$$+\frac{M_{LL}^{(4)}}{(x\,P_1 + (1-y)P_2 - u\,P_B^+)^2 - m_q^2 + i\epsilon}]\}.$$

For example, the explicit expression for the hadronic matrix element of the factorizable emission contributions for the $(V-A)\times(V-A)$ effective four-quark vertexes:

$$\begin{aligned} T_{LLa}^{FM_1M_2}(M) &= i\frac{1}{4}\frac{C_F}{N_C}\, F_M\, F_{M_1}\, F_{M_2}\int_0^1\int_0^1\int_0^1 du\, dx\, dy\, m_B^2\phi_M(u) \\ &\quad \Big\{m_B(2m_b - m_B x)\phi_{M_1}(x) + \mu_{M_1}(2m_B x - m_b) \\ &\quad [\phi_{M_1}^p(x) - \phi_{M_1}^T(x)]\Big\}\phi_{M_2}(y)h_{Ta}^F(u,x), \end{aligned}$$

The functions $h^F(u,x)_{TA}$ arise from propagators of gluon and quark and has the following explicit form:

$$h_{Ta}^F(u,x) = \frac{1}{(-u(1-x)m_B^2 - \mu_g^2 + i\epsilon)(xm_B^2 - m_b^2 + i\epsilon)},$$

Nonperturbative Corrections I: Emission Diagrams

The vertex corrections were proposed to improve the scale dependence of Wilson coefficient functions of factorizable emission amplitudes in QCDF. Those coefficients are always combined as $C_{2n-1}+\frac{C_{2n}}{N_C}$ and $C_{2n}+\frac{C_{2n-1}}{N_C}$, which, after taken into account the vertex corrections, are modified to:

$$C_{2n-1}(\mu)+\frac{C_{2n}}{N_C}(\mu)\to C_{2n-1}(\mu)+\frac{C_{2n}}{N_C}(\mu)+\frac{\alpha_s(\mu)}{4\pi}C_F\frac{C_{2n}(\mu)}{N_c}V_{2n-1}(M_2)\,,$$
$$C_{2n}(\mu)+\frac{C_{2n-1}}{N_C}(\mu)\to C_{2n}(\mu)+\frac{C_{2n-1}}{N_C}(\mu)+\frac{\alpha_s(\mu)}{4\pi}C_F\frac{C_{2n-1}(\mu)}{N_c}V_{2n}(M_2)\,,$$

with $n=1,...,5$, M_2 being the meson emitted from the weak vertex.In the naive dimensional regulation (NDR) scheme, $V_i(M)$ are given by:

$$V_i(M) \;=\; \begin{cases} 12\ln(\frac{m_b}{\mu})-18+\int_0^1 dx\,\phi_a(x)\,g(x)\,, & \text{for } i=1-4,9,10\,,\\ -12\ln(\frac{m_b}{\mu})+6-\int_0^1 dx\,\phi_a(1-x)\,g(1-x)\,, & \text{for } i=5,7\,,\\ -6+\int_0^1 dx\,\phi_b(x)\,h(x)\,, & \text{for } i=6,8\,, \end{cases}$$

where $\phi_a(x)$ and $\phi_b(x)$ denote the leading-twist and twist-3 distribution amplitudes for a pseudoscalar meson or a longitudinally polarized vector meson, respectively.

To further improve our predictions, we shall examine an interesting case that vertexes receive additional large non-perturbative contributions, namely the Wilson coefficients $a_i = C_i + \frac{C_{i\pm1}}{N_C}$ are modified to be the following effective ones:

$$a_i \to a_i^{eff} = C_i(\mu) + \frac{C_{i\pm1}}{N_C}(\mu) + \frac{\alpha_s(\mu)}{4\pi} C_F \frac{C_{i\pm1}(\mu)}{N_c}(V_i(M_2) + \widetilde{V}_1(M_2)) , \qquad (i = 1-4, 9, 10)$$

$$a_i \to a_i^{eff} = C_i(\mu) + \frac{C_{i\pm1}}{N_C}(\mu) + \frac{\alpha_s(\mu)}{4\pi} C_F \frac{C_{i\pm1}(\mu)}{N_c}(V_i(M_2) + \widetilde{V}_2(M_2)) , \qquad (i = 5-8)$$

The corrections $\widetilde{V}_1(M_2)$ and $\widetilde{V}_2(M_2)$ depend on whether the meson M_2 is a pseudoscalar or a vector. It could be caused from the higher order non-perturbative non-local effects. Adopting $\widetilde{V}_1(P) = 26e^{-\frac{\pi}{3}i}$, $\widetilde{V}_2(P) = -26$, $\widetilde{V}_1(V) = 15e^{\frac{\pi}{8}i}$, and $\widetilde{V}_2(V) = -15e^{\frac{\pi}{8}i}$, both the branching ratios and CP asymmetries of most $B \to PP, PV, VV$ decay modes are improved.

Nonperturbative Corrections II:Annihilation Diagrams

Most of the annihilation contributions are from factorizable annihilation diagrams with the $(S-P)\times(S+P)$ effective four-quark vertex:

$$A_{SP}^{P_1P_2}(M) \sim \int dxdy \frac{(\mu_{P_1}+\mu_{P_2})y(1-y)}{(x(1-y)m_B^2-\mu_g^2+i\epsilon)((1-y)m_B^2-m_q^2+i\epsilon)},$$

$$A_{SP}^{P_1V_2}(M) \sim \int dxdy \frac{(\mu_{P_1}-3(2x-1)m_{V_2})y(1-y)}{(x(1-y)m_B^2-\mu_g^2+i\epsilon)((1-y)m_B^2-m_q^2+i\epsilon)},$$

$$A_{SP}^{V_1P_2}(M) \sim \int dxdy \frac{(-3(1-2x)m_{V_1}-\mu_{P_2})y(1-y)}{(x(1-y)m_B^2-\mu_g^2+i\epsilon)((1-y)m_B^2-m_q^2+i\epsilon)},$$

$$A_{SP}^{V_1V_2}(M) \sim \int dxdy \frac{3(1-2x)(-m_{V_1}+3(2x-1)m_{V_2})y(1-y)}{(x(1-y)m_B^2-\mu_g^2+i\epsilon)((1-y)m_B^2-m_q^2+i\epsilon)}.$$

1. Since the contributions of these amplitudes are dominated by the area $x\sim 0$ or $y\sim 1$, $A_{SP}^{P_1P_2}(M)$ and $A_{SP}^{P_1V_2}(M)$ have the same sign, while $A_{SP}^{V_1P_2}(M)$ and $A_{SP}^{V_1V_2}(M)$ have a different sign from $A_{SP}^{P_1P_2}(M)$
2. As a result, we use the same strong phase for $A_{SP}^{P_1P_2}(M)$ and $A_{SP}^{P_1V_2}(M)(\theta_1^a\sim 5^o)$, and another one for $A_{SP}^{V_1P_2}(M)$ and $A_{SP}^{V_1V_2}(M)(\theta_1^a\sim 60^o)$.

Input Parameters

1. Light-cone distribution amplitudes
2. CKM Matrix Elements,Decay constants *etc.*
3. Running scale, cut-off scale
4. Strong Phases

Light-cone distribution amplitudes

1. **B meson wave function**

   For the B-meson wave function, we take the following standard form in our numerical calculations:

$$\phi_B(x) \quad = \quad N_B x^2(1-x)^2 \exp\left[-\frac{1}{2}\left(\frac{x m_B}{\omega_B}\right)^2\right] ,$$

   where the shape parameter of B meson is $\omega_B = 0.25 GeV$, and N_B is a normalization constant.

1 Light mesons

The light-cone distribution amplitudes (LCDAs) for pseudoscalar and vector mesons are as below:

- twist-2

$$\begin{aligned}
\phi_P(x,\mu) &= 6x(1-x)\big[1+\sum_{n=1}^{\infty} a_n^P(\mu) C_n^{3/2}(2x-1)\big], \\
\phi_V(x,\mu) &= 6x(1-x)\big[1+\sum_{n=1}^{\infty} a_n^V(\mu) C_n^{3/2}(2x-1)\big], \\
\phi_V^T(x,\mu) &= 6x(1-x)\big[1+\sum_{n=1}^{\infty} a_n^{T,V}(\mu) C_n^{3/2}(2x-1)\big],
\end{aligned}$$

- twist-3

$$\begin{aligned}
\phi_p(x,\mu) &= 1, \qquad \phi_\sigma(x,\mu) = 6x(1-x), \\
\phi_\nu(x,\mu) &= 3\big[2x-1+\sum_{n=1}^{\infty} a_n^{T,V}(\mu) P_{n+1}(2x-1)\big] \\
\phi_+(x) &= 3(1-x)^2, \qquad \phi_-(x) = 3x^2,
\end{aligned}$$

CKM Matrix Elements, Hadronic Input Parameters and Decay constants

As for the CKM matrix elements, we use the Wolfenstein parametrization with the four parameters chosen as:

$$A = 0.798^{+0.023}_{-0.017},\ \lambda = 0.2252^{+0.00083}_{-0.00082},\ \bar{\rho} = 0.141^{+0.035}_{-0.021},\ \bar{\eta} = 0.340 \pm 0.016$$

And the hadronic input parameters and the decay constants taken from the QCD sum rules and Lattice theory are as below:

$\tau_{B^\pm}$	τ_{B_d}	m_B	m_b	m_t	m_u	m_d
1.638ps	1.525ps	5.28GeV	4.4GeV	173.3GeV	4.2MeV	7.6MeV
m_c	m_s	$m_{\pi^\pm}$	m_{π^0}	m_K	m_{ρ^0}	$m_{\rho^\pm}$
1.5GeV	0.122GeV	0.140GeV	0.135GeV	0.494GeV	0.775GeV	0.775GeV
m_ω	m_ϕ	$m_{K^{*\pm}}$	$m_{K^{*0}}$	μ_π	μ_K	f_ϕ
1.7GeV	1.8GeV	300MeV	0.78GeV	1.02GeV	0.892GeV	0.215GeV
f_B	f_π	f_K	f_ρ	f_ω	f_{K^*}	f_ω^T
0.210GeV	0.130GeV	0.16GeV	0.216GeV	0.187GeV	0.220GeV	0.151GeV
$f_{K^*}^T$	f_ϕ^T	f_ρ^T				
0.185GeV	0.186GeV	0.165GeV				

1. **Running scale**
   In our numerical calculations, the running scale is taken to be

$$\mu = 1.5 \pm 0.1\mathrm{GeV} \sim \sqrt{2\Lambda_{QCD} m_b}.$$

   The scale of $\alpha_s(\mu)$ in the six-quark operator effective Hamiltonian is also taken at $\mu = 1.5 GeV$. Mass of b quark running to $\mu = 1.5 \pm 0.1\ GeV$ is $m_b(\mu) \simeq 5.54 GeV$.

2. **Cut-off scale**
   The infrared cut-offs for gluon and light quarks are the basic scale to determine annihilation diagram contributions and are set to be $\mu_q = \mu_g = 0.37 GeV$.

Strong phases

- In general, a Feynman diagram will yield an imaginary part for the decay amplitudes when the virtual particles in the diagram become on mass-shell,which generates the strong phase of the process and the resulting diagram can be considered as a genuine physical process.
- The calculation of strong phase from nonperturbative QCD effects is a hard task, there exist no efficient approaches to evaluate reliably the strong phases caused from nonperturbative QCD effects, so we set the strong phase as an input parameter in our framework.
- We adopt different strong phases of annihilation diagrams θ^a in $B \to PP, PV, VV$ decay modes respectively to get the reasonable results.

Numerical Calculation: Form factors

The method developed based on the six quark effective Hamiltonian allows us to calculate the relevant transition form factors via a simple factorization approach. They are calculated by the following formalisms

$$F_0^{B\to M_1} = \frac{4\pi\alpha(\mu)C_F}{N_c m_B^2 F_{M_2}} T_{LL}^{FM_1M_2}(B)(M_1, M_2 = P),$$

$$V^{B\to M_1} = \frac{4\pi\alpha(\mu)C_F}{N_c m_B^2 F_{M_2}} T_{LL,\perp}^{FM_1M_2}(B) \frac{m_B^2(m_B + m_{M_1})}{m_{M_2}(m_B^2 - m_{M_1} m_{M_2})}(M_1, M_2 = V),$$

$$A_0^{B\to M_1} = \frac{4\pi\alpha(\mu)C_F}{N_c m_B^2 F_{M_2}} T_{LL}^{FM_1M_2}(B)(M_1 = V, M_2 = P),$$

$$A_1^{B\to M_1} = \frac{4\pi\alpha(\mu)C_F}{N_c m_B^2 F_{M_2}} T_{LL,//}^{FM_1M_2}(B) \frac{m_B^2}{m_{M_2}(m_B + m_{M_1})}(M_1, M_2 = V)$$

with:

$$T_{LL,\perp} = \frac{1}{2}(T_{LL,+} - T_{LL,-}), \qquad C_F = \frac{N_c^2 - 1}{2N_c},$$

Table: *The $B \to P, V$ form factors at $q^2 = 0$ in QCD Sum Rules, Light Cone and our work.*

Mode	F(0)	QCDSR	LC	LC(HQEFT)	PQCD	**This work**
$B \to K^*$	V	0.411	0.339	0.331	0.406	0.277
	A_0	0.374	0.283	0.280	0.455	0.328
	A_1	0.292	0.248	0.274	0.30	0.220
$B \to \rho$	V	0.323	0.298	0.289	0.318	0.233
	A_0	0.303	0.260	0.248	0.366	0.280
	A_1	0.242	0.227	0.239	0.25	0.193
$B \to \omega$	V	0.293	0.275	0.268	0.305	0.206
	A_0	0.281	0.240	0.231	0.347	0.251
	A_1	0.219	0.209	0.221	0.30	0.170
$B \to \pi$	F_0	0.258	0.247	0.285	0.292	0.269
$B \to K$	F_0	0.331	0.297	0.345	0.321	0.349

Amplitudes of charmless B Decays

Take $B \to \pi\pi$ decay as example,the decay amplitudes can be expressed as follows:

$$
\begin{aligned}
A(B^0 \to \pi^+\pi^-) &= V_{td}V_{tb}^*[P_T^{\pi\pi}(B) + \frac{2}{3}P_{EW}^{C\pi\pi}(B) + P_E^{\pi\pi}(B) + 2P_A^{\pi\pi}(B) \\
&\quad + \frac{1}{3}P_{EW}^{A\pi\pi}(B) - \frac{1}{3}A_{EW}^{E\pi\pi}(B)] - V_{ud}V_{ub}^*[T^{\pi\pi}(B) + E^{\pi\pi}(B)], \\
A(B^+ \to \pi^+\pi^0) &= \frac{1}{\sqrt{2}}\{V_{td}V_{tb}^*[P_{EW}^{\pi\pi}(B) + P_{EW}^{C\pi\pi}(B)] - V_{ud}V_{ub}^*[T^{\pi\pi}(B) + C^{\pi\pi}(B)]\}, \\
A(B^0 \to \pi^0\pi^0) &= \frac{1}{\sqrt{2}}\{-V_{td}V_{tb}^*[P_T^{\pi\pi}(B) - P_{EW}^{\pi\pi}(B) - \frac{1}{3}P_{EW}^{C\pi\pi}(B) + P_E^{\pi\pi}(B) \\
&\quad + 2P_A^{\pi\pi}(B) + \frac{1}{3}P_{EW}^{A\pi\pi}(B) - \frac{1}{3}P_{EW}^{E\pi\pi}(B)] \\
&\quad + V_{ud}V_{ub}^*[-C^{\pi\pi}(B) + E^{\pi\pi}(B)]\},
\end{aligned}
$$

Totally,there're 11 amplitudes, which are defined as follows:

$$
\begin{aligned}
T^{M_1M_2}(M) &= 4\pi\alpha_s(\mu)\frac{G_F}{\sqrt{2}}\{[C_1(\mu)+\frac{1}{N_C}C_2(\mu)]T_{LL}^{FM_1M_2}(M) \\
&\quad +\frac{1}{N_C}C_2(\mu)T_{LL}^{NM_1M_2}(M)\}, \\
C^{M_1M_2}(M) &= 4\pi\alpha_s(\mu)\frac{G_F}{\sqrt{2}}\{[C_2(\mu)+\frac{1}{N_C}C_1(\mu)]T_{LL}^{FM_1M_2}(M) \\
&\quad +\frac{1}{N_C}C_1(\mu)T_{LL}^{NM_1M_2}(M)\}, \\
P_{EW}^{M_1M_2}(M) &= 4\pi\alpha_s(\mu)\frac{G_F}{\sqrt{2}}\frac{3}{2}\{[C_9(\mu)+\frac{1}{N_C}C_{10}(\mu)]T_{LL}^{FM_1M_2}(M) \\
&\quad +\frac{1}{N_C}C_{10}(\mu)T_{LL}^{NM_1M_2}(M)+[C_7(\mu)+\frac{1}{N_C}C_8(\mu)]T_{LR}^{FM_1M_2}(M) \\
&\quad +\frac{1}{N_C}C_8(\mu)T_{SP}^{NM_1M_2}(M)\}, \\
&\cdots\cdots
\end{aligned}
$$

Numerical results for B to PP decays

Table: The branching ratios (in units of 10^{-6}) and direct CP asymmetries in $B \to \pi K$ decays. The central values are obtained at $\mu_q = \mu_g$=0.37GeV.*(Penguin dominate)*

Mode	Data[HFAG]	This work				
		NLO+Vertex	NLO^{eff}	NLO^{eff} (-10°)	NLO^{eff} (5°)	NLO^{eff} (20°)
$B^+ \to \pi^+ K^0$	23.1 ± 1.0	22.5	21.4	19.0	22.6	25.9
$B^+ \to \pi^0 K^+$	12.9 ± 0.6	12.8	12.5	11.2	13.1	14.9
$B^0 \to \pi^- K^+$	19.4 ± 0.6	19.2	19.5	17.4	20.5	23.3
$B^0 \to \pi^0 K^0$	9.8 ± 0.6	8.3	8.4	7.4	8.9	10.2
$A_{CP}(\pi^+ K^0)$	0.009 ± 0.025	-0.006	-0.006	-0.006	-0.007	-0.007
$A_{CP}(\pi^0 K^+)$	0.050 ± 0.025	-0.053	0.012	0.003	0.018	0.034
$A_{CP}(\pi^- K^+)$	-0.098 ± 0.012	-0.118	-0.139	-0.158	-0.131	-0.105
$A_{CP}(\pi^0 K^0)$	-0.01 ± 0.10	-0.052	-0.139	-0.143	-0.138	-0.137
$S_{\pi^0 K_S}$	0.58 ± 0.17	0.699	0.760	0.768	0.756	0.745

Table: $B \to \pi\pi, KK$ decay modes *(Tree dominate)*

Mode	Data[HFAG]	This work				
		NLO+Vertex	NLO^{eff}	NLO^{eff} (-40°)	NLO^{eff} (5°)	NLO^{eff} (50°)
$B^0 \to \pi^-\pi^+$	5.16 ± 0.22	7.1	6.5	6.00	6.6	7.6
$B^+ \to \pi^+\pi^0$	5.59 ± 0.40	4.1	5.5	5.51	5.5	5.5
$B^0 \to \pi^0\pi^0$	1.55 ± 0.19	0.3	1.0	1.11	1.0	1.0
$B^+ \to K^+\bar{K}^0$	1.36 ± 0.28	1.7	1.6	1.0	1.7	2.2
$B^0 \to K^0\bar{K}^0$	0.96 ± 0.20	1.5	1.4	0.7	1.5	2.2
$B^0 \to K^+K^-$	0.15 ± 0.10	0.09	0.09	0.09	0.09	0.09
$A_{CP}(\pi^-\pi^+)$	0.38 ± 0.06	0.206	0.266	0.239	0.260	0.141
$A_{CP}(\pi^+\pi^0)$	0.06 ± 0.05	-0.000	-0.001	-0.001	-0.001	-0.001
$A_{CP}(\pi^0\pi^0)$	0.43 ± 0.25	0.382	0.453	0.272	0.485	0.789
$S_{\pi\pi}$	-0.61 ± 0.08	-0.504	-0.506	-0.353	-0.524	-0.638
$A_{CP}(K^+\bar{K}^0)$	0.12 ± 0.17	0.101	0.098	0.041	0.101	0.106
$A_{CP}(K^0\bar{K}^0)$	-0.58 ± 0.7	0.000	0.000	0.000	0.000	0.000
$A_{CP}(K^+K^-)$	-	-0.184	-0.184	-0.184	-0.184	-0.184

Numerical results for B to PV decays

Table: The branching ratios (in units of 10^{-6}) and direct CP asymmetries in penguin dominated $B \to PV$ decays

Mode	Data[HFAG]	This work				
		NLO+Vertex	NLO^{eff}	NLO^{eff} (-10°)	NLO^{eff} (5°)	NLO^{eff} (20°)
$B^+ \to K^{*0}\pi^+$	9.9 ± 0.8	10.3	9.0	7.6	9.8	11.8
$B^+ \to K^{*+}\pi^0$	6.9 ± 2.3	6.2	5.5	4.8	5.9	7.1
$B^0 \to K^{*-}\pi^+$	8.6 ± 0.9	8.8	8.3	7.2	8.9	10.6
$B^0 \to K^{*0}\pi^0$	2.4 ± 0.7	3.5	3.6	3.1	3.9	4.6
$B^+ \to \phi K^+$	8.30 ± 0.65	9.3	6.9	5.6	7.6	9.6
$B^0 \to \phi K^0$	8.3 ± 1.1	8.9	6.6	5.4	7.3	9.2
$A_{CP}(K^{*0}\pi^+)$	-0.038 ± 0.042	-0.017	-0.018	-0.020	-0.017	-0.015
$A_{CP}(K^{*+}\pi^0)$	0.04 ± 0.29	-0.224	-0.123	-0.164	-0.103	-0.045
$A_{CP}(K^{*-}\pi^+)$	-0.23 ± 0.08	-0.357	-0.355	-0.415	-0.327	-0.251
$A_{CP}(K^{*0}\pi^0)$	-0.15 ± 0.12	-0.067	-0.125	-.114	-0.129	-0.143
$A_{CP}(\phi K^+)$	0.23 ± 0.15	-0.022	-0.025	-0.028	-0.023	-0.020
$A_{CP}(\phi K^0)$	-0.01 ± 0.06	0	0	0	0	0

Mode	Data[HFAG]	This work				
		NLO+Vertex	NLO^{eff}	NLO^{eff} (45°)	NLO^{eff} (60°)	NLO^{eff} (75°)
$B^+ \to \rho^+ K^0$	8.0 ± 1.45	5.2	7.1	7.1	6.8	6.3
$B^+ \to \rho^0 K^+$	3.81 ± 0.48	3.0	3.3	2.8	2.6	2.4
$B^0 \to \rho^- K^+$	8.6 ± 1.0	5.4	6.2	7.3	7.3	7.2
$B^0 \to \rho^0 K^0$	4.7 ± 0.7	2.8	3.9	4.9	5.0	5.0
$B^+ \to \omega K^+$	6.7 ± 0.5	2.4	3.6	4.3	5.3	5.2
$B^0 \to \omega K^0$	5.0 ± 0.6	1.9	3.2	4.1	4.8	4.6
$A_{CP}(\rho^+ K^0)$	-0.12 ± 0.17	0.016	0.013	0.014	0.014	0.014
$A_{CP}(\rho^0 K^+)$	0.37 ± 0.11	0.635	0.727	0.594	0.463	0.285
$A_{CP}(\rho^- K^+)$	0.15 ± 0.06	0.605	0.549	0.373	0.290	0.196
$A_{CP}(\rho^0 K^0)$	0.06 ± 0.20	0.056	-0.136	-0.044	-0.015	0.015
$A_{CP}(\omega K^+)$	0.02 ± 0.05	0.453	0.404	0.167	0.091	0.015
$A_{CP}(\omega K^0)$	0.32 ± 0.17	-0.011	0.117	0.048	0.026	0.002

Table: Tree dominant $B \to PV$ decay modes

Mode	Data[HFAG]	This work					
		NLO+Vertex	NLO^{eff}				
			default	$(-45^{\circ},0^{\circ})$	$(45^{\circ},0^{\circ})$	$(0^{\circ},-45^{\circ})$	$(0^{\circ},45^{\circ})$
$B^+ \to \rho^+\pi^0$	10.9 ± 1.5	12.0	13.9	14.2	13.5	13.7	14.2
$B^+ \to \rho^0\pi^+$	8.3 ± 1.3	5.2	7.4	7.0	7.8	7.2	7.4
$B^0 \to \rho^+\pi^-$	15.7 ± 1.8	19.6	17.4	16.5	19.1	17.5	17.4
$B^0 \to \rho^-\pi^+$	7.3 ± 1.2	6.2	6.5	6.5	6.5	6.1	7.5
$B^0 \to \rho^0\pi^0$	2.0 ± 0.5	0.2	1.3	1.5	1.2	1.5	1.1
$B^+ \to \bar{K}^{*0}K^+$	0.68 ± 0.19	0.6	0.3	0.3	0.3	0.3	0.3
$B^0 \to K^{*0}\bar{K}^0$	< 1.9	0.6	0.4	0.2	0.8	0.8	0.1
$A_{CP}(\rho^+\pi^0)$	0.02 ± 0.11	0.255	0.199	0.196	0.133	0.195	0.131
$A_{CP}(\rho^0\pi^+)$	$0.18^{+0.09}_{-0.17}$	-0.308	-0.344	-0.330	-0.269	-0.309	-0.285
$A_{CP}(\rho^+\pi^-)$	0.11 ± 0.06	0.120	0.126	0.108	0.066	0.121	0.127
$A_{CP}(\rho^-\pi^+)$	-0.18 ± 0.12	-0.281	-0.282	-0.283	-0.281	-0.217	-0.176
$A_{CP}(\rho^0\pi^0)$	-0.30 ± 0.38	0.058	0.187	0.112	0.381	0.258	-0.008
$A_{CP}(\bar{K}^{*0}K^+)$	-	0.191	0.257	-0.342	0.205	0.112	0.837
$A_{CP}(k^{*0}\bar{K}^0)$	-	0.000	0	0	0	0	0

Numerical results for B to VV decays

Table: Branching ratios for $B \to VV$ decay modes (in unit of 10^{-6}) which includes the contribution of effective Wilson coefficients and effect of different strong phase $\theta^a = 60^\circ \pm 15^\circ$) for annihilation diagram.

Mode	Data[HFAG]	This work				
		NLO+Vertex	NLO^{eff}	NLO^{eff} (45°)	NLO^{eff} (60°)	NLO^{eff} (75°)
$B^+ \to \rho^+\rho^0$	24.0 ± 2.0	13.4	16.8	16.8	16.8	16.8
$B^0 \to \rho^+\rho^-$	24.2 ± 3.1	22.3	19.8	21.7	22.3	22.7
$B^0 \to \rho^0\rho^0$	0.73 ± 0.27	0.4	0.92	0.67	0.61	0.57
$B^+ \to K^{*0}\rho^+$	9.2 ± 1.5	16.2	14.0	9.6	8.3	7.2
$B^+ \to K^{*+}\rho^0$	< 6.1	9.9	9.0	6.4	5.6	5.0
$B^0 \to K^{*+}\rho^-$	< 12	13.9	13.0	9.1	7.9	6.9
$B^0 \to K^{*0}\rho^0$	3.4 ± 1.0	5.6	5.2	3.6	3.1	2.7
$B^+ \to \bar{K}^{*0}K^{*+}$	1.2 ± 0.5	0.9	0.8	0.6	0.5	0.4
$B^0 \to \bar{K}^{*0}K^{*0}$	1.28 ± 0.35	0.8	0.6	0.5	0.5	0.5
$B^0 \to K^{*+}K^{*-}$	< 2	0.07	0.07	0.07	0.007	0.07
$B^+ \to \phi K^{*+}$	10.0 ± 1.1	19.4	15.2	10.9	9.5	8.4
$B^0 \to \phi K^{*0}$	9.8 ± 0.7	18.7	14.8	10.5	9.2	8.1
$B^+ \to \omega K^{*+}$	< 7.4	5.6	4.2	3.3	3.0	2.8
$B^0 \to \omega K^{*0}$	2.0 ± 0.5	6.2	4.1	2.8	2.5	2.2

Conclusions

- Based on the approximate six-quark operator effective Hamiltonian derived from perturbative QCD, the QCD factorization approach has been naturally applied to evaluate the hadronic matrix elements for charmless two body B-meson decays. It is shown that, with annihilation contribution and extra strong phase, our framework provides a simple way to evaluate the hadronic matrix elements of two body decays.
- For $B \to PP$ final states, our predictions for branching ratios and CP asymmetries are generally consistent with the current experimental data within their respective uncertainties, once the effective Wilson coefficients and annihilation amplitude with small strong phase ($\theta^a = 5^\circ$) are adopted. Especially for the branching ratio of $B \to \pi^0\pi^0$ mode, our result, although being still smaller than the data, is consistent with that in QCDF.

- As for $B \to PV$ decays, similar conclusions are found. The exceptions here are the branching ratio of $\rho^+\pi^0$ and $B \to K^{*0}\pi^0$ modes, which are bigger than the data. An interesting point should be noted that our predictions are also consistent with the ones in QCDF. Since the current data on CP asymmetries have large uncertainties in these modes, more precise experimental data are expected to further test our framework.
- In $B \to VV$ decay modes, we have shed light on the polarization anomalies observed in $B \to \phi K^*, \rho K^*, \omega K^*$ decays. It is noted that these anomalies could be explained in our framework when considering annihilation contributions with a big strong phase ($\theta^a = 60^\circ$). Moreover, the annihilation contributions with a strong phase have remarkable effects on the branching ratios and CP asymmetries, especially on the observables of penguin dominated decay modes.

Discussions

- It is noted that the method developed in this paper allows us to calculate the relevant transition **form factors**. Our predictions(for B to light mesons form factors) are consistent with the results of light-core QCD sum-rules and pQCD.
- A complete six-quark operator effective Hamiltonian may involve more effective operators from the type III diagrams and lead to a non-negligible contribution to hadronic B meson decays when evaluating the hadronic matrix elements of six quark operator effective Hamiltonian around the energy scale $\mu \sim \sqrt{2\Lambda_{QCD} m_b} \sim m_c \sim 1.5$ GeV where the nonperturbative effects may play the role.
- Through this approach, we find that the factorization is a natural result and it is more clear to see what approximation is made(such as the Type III diagrams), which makes the physics of long-distance contribution much understandable.
- For the calculation of strong phase from nonperturbative QCD effects is a hard task, and there exist no efficient approaches to evaluate reliably the strong phases caused from nonperturbative QCD effects, they are treated as free parameters in this frame work, and the values differ for different decay modes in order to get reasonable predictions.

Thanks for attention!